Apparent viscosity of *p*-methoxybenzylidene-*p′*-*n*-butylaniline in the presence of electrohydrodynamic convection

Tomoyuki Nagaya* and Mikiyasu Niu
Department of Electrical and Electronic Engineering, Faculty of Engineering, Oita University, Oita 870-1192, Japan

Shigetoshi Nara†
Division of Industrial Innovation Sciences, Graduate School of Natural Science and Technology, Okayama University, 3-1-1 Tsushimanaka Okayama 700-8530, Japan

Yang Ho Na‡
Department of Advanced Materials, College of Life Science and Nano Technology, Hannam University, Daejeon 305-811, South Korea

Hiroshi Orihara§
Department of Applied Physics, Graduate School of Engineering, Hokkaido University, Sapporo 060-8628, Japan
(Received 23 June 2012; published 8 January 2013)

The apparent shear viscosity of *p*-methoxybenzylidene-*p′*-*n*-butylaniline in the presence of electrohydrodynamic convection (EHC) is investigated experimentally. In the absence of an electric field, directors are almost aligned along the flow direction such that the viscosity is close to the minimum of the Miesowicz viscosities. Since EHC disturbs the flow-aligned director configuration, the viscosity increases as the applied voltage is increased in the low-voltage regime. In the high-voltage regime, however, further increasing the voltage leads to a decrease in viscosity. Microscope observations using a rheometer reveal that the decrease in viscosity occurs in the dynamic scattering mode 2 (DSM2) state, whose spatial director distribution is anisotropic due to the shear flow. By adopting the Ericksen-Leslie theory for the shear flow under the electric field, we find that the viscosity decrease can be attributed to the negative contribution of the electric stress caused by the anisotropic director distribution of the DSM2 state.

DOI: 10.1103/PhysRevE.87.012501 PACS number(s): 83.80.Xz, 83.60.Np, 47.65.Gx

I. INTRODUCTION

Electrohydrodynamics convection (EHC) [1] is observed in nematic liquid crystals with negative dielectric anisotropy ($\varepsilon_a < 0$). Because of the richness of its bifurcation phenomena, EHC has received considerable attention over the past 2 decades [2]. In the field of rheology, the electrorheological (ER) effect in liquid crystals—namely the reversible change of apparent viscosity due to the application of an electric field—is of particular interest in terms of its mechanical applications [3–14]. The viscosity of rodlike nematics under a shear flow varies depending on the relative orientation of the director **n** (average direction of the long axis of molecules), the flow direction and the velocity gradient of the flow, which is known as the anisotropy of viscosity [15]. Since the ER effect in liquid crystals is attributed to the reorientation of rodlike molecules by virtue of the electric torque from the flow-aligned director configuration under no electric field, the magnitude of the ER response is determined essentially by the values of the Miesowicz viscosities η_2 and η_1 [15] that represent the viscosities when the director is parallel to the flow and to the velocity gradient of the flow, respectively. Normally, positive ER effect, i.e., the increase of viscosity by the electric field, is hoped for and η_1 is larger than η_2 for the most rodlike nematics. Accordingly, liquid crystals of positive dielectric anisotropy have predominantly been examined [3–12] because the increase of viscosity from η_2 to η_1 seems to be obtained easily when the electric field is applied on the liquid crystal perpendicularly to the flow direction. Although the magnitude of the ER effect for low-molecular-weight nematics with positive dielectric anisotropy is not enough for general mechanical applications except for micromachines, liquid crystal polymer dissolved in a nematic solvent [10] and LC polymer solution [4] show potential for exhibiting a substantial ER effect. In contrast, the ER effect in liquid crystals with negative dielectric anisotropy has been less studied because it is not easy to obtain the increase of viscosity from η_2 to η_1 in simple experimental geometries. However, if the ER effect in liquid crystals with negative dielectric anisotropy is caused by the appearance of EHC, the study of the ER effect is very important from the viewpoint of the influence of dissipative structures on the transportation phenomena in a nonequilibrium open system. In addition, since the dissipative structures are investigated extensively in various fields of natural science and engineering, the knowledge of the rheology of liquid crystal under the EHC state is worthy beyond the material physics of liquid crystals.

The apparent viscosity of *p*-methoxybenzylidene-*p′*-*n*-butylaniline (MBBA), which is a typical liquid crystal displaying EHC, under dc and ac fields was first investigated by Honda *et al.* [13] from the viewpoint of the ER effect. They

*nagaya@oita-u.ac.jp
†nara@elec.okayama-u.ac.jp
‡yhna@hnu.kr
§orihara@eng.hokudai.ac.jp

anticipated that MBBA's apparent viscosity is increased by the turbulent flow induced by the electric field, the so-called *dynamic scattering mode* (DSM) [1,2], and confirmed their prediction experimentally using a Tsuda viscometer. However, the following important feature of the apparent viscosity under high ac voltages was not addressed in their report: It increased up to a characteristic voltage V_{peak} and above V_{peak} decreased with increasing applied voltage. In 1995, Negita [14] attempted to corroborate Honda *et al.*'s [13] experiments using a custom-made viscometer constructed from concentric double cylinders with gap $d = 1$ mm and obtained completely different results. In contrast to Honda *et al.*, MBBA's apparent viscosity under an ac current of 100 Hz was found to monotonically decrease when the electric field was below 2 kV/mm and to saturate at a constant value when the electric field was greater than this. However, Negita did not dismiss Honda *et al.*'s results because they were unable to establish EHC in their experiments.

The convective flow of nematic molecules is induced by the drag force from moving charges that are driven by the ac field. The charges, positive and negative ions created by dissociation of the MBBA molecule, always present in the sample [16]. When the frequency of the electric field, f, is higher than the frequency of charge relaxation, these cannot move. This characteristic frequency, the so-called *cut-off frequency* f_{c}, decreases as the liquid's conductivity decreases [17]. The frequency regimes for $f < f_{\mathrm{c}}$ and $f_{\mathrm{c}} < f$ are called "conduction" and "dielectric" regimes, respectively. In the dielectric regime, a fine oscillatory striation pattern ("chevron") appears at a certain threshold of the electric field that is order of 25 kV/cm for $f = 100$ Hz [18]. Experimentally, it is known that the chevron is not convection over the whole volume of the sample but a skin convection just close to the electrodes [19,20]. Hence, we contend that f_{c} for Negita's sample was less than 100 Hz such that no convection over the whole volume of the sample was induced. Since there was no anomaly in the apparent viscosity above 2 kV/mm, we infer that the chevron pattern did not appear in his sample, otherwise it appeared but it did not influence the apparent viscosity. Although no MBBA sample in either experiment was doped with an ionic compound, the conductivities of the samples might not be of the same order because weak dissociation of molecules into ions cannot be controlled [16]. Therefore, to investigate the apparent viscosity under various EHC states, MBBA should be doped with a suitable amount of ionic compound.

To the best of our knowledge, the decrease in MBBA's apparent viscosity under a well-developed turbulent state induced by a high electric voltage remains an open question. The aim of the present paper is, thus, to characterize the features of this phenomenon experimentally and to investigate its origin. To discuss the relation between MBBA's apparent viscosity and the orientational order of molecules in the sample, viscosity measurements, and microscope observations are performed simultaneously by using a rheometer consisting of transparent parallel plates.

This paper is organized as follows. In the next section, the experimental setup is briefly described. In Sec. III, the results of our experiments are presented and discussed. The last section then provides a summary of this work.

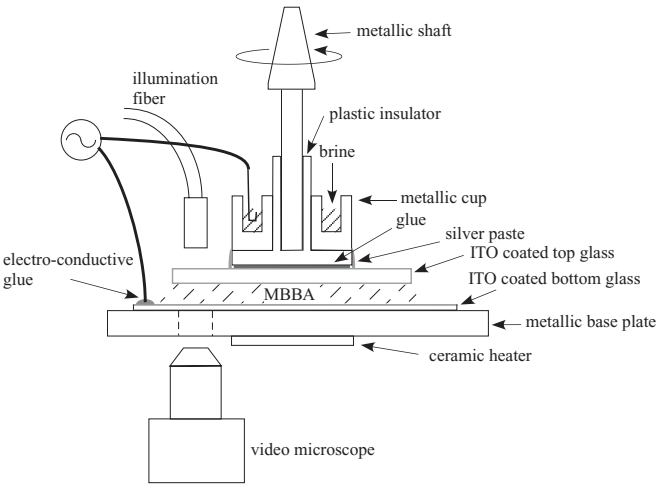

FIG. 1. Schematic diagram of sensor.

II. EXPERIMENTAL SETUP

To ensure the induction of EHC, MBBA was doped with an ionic compound, tetra-*n*-butylammonium bromide (TBAB), at a concentration of 0.00063 wt%. The steady-shear viscosity of this sample was then measured between the parallel plates of a stress-controlled rheometer (HAAKE RS-75). We also constructed a sensor for the rheometer to observe the sample by coating a pair of glass plates with indium tin oxide (ITO). The structure of the sensor system is shown schematically in Fig. 1. The upper part of the sensor consists of a metallic shaft, a plastic insulator, a metallic cup, and a circular glass plate, and the lower part consists of a glass plate, a metallic base plate, and thin ceramic heaters. The entire surface of the upper glass plate and the upper surface of the lower glass plate were coated with ITO; however, an anchoring treatment was not applied to any of the surfaces. The diameter and thickness of the upper glass plate were 60 and 5 mm, respectively. The size and thickness of the lower glass plate were 90×90 mm and 1.1 mm, respectively. The gap between the glass plates was fixed at $d = 100$ μm.

The metallic cup, which was filled with brine, was brought into electrical contact with the upper glass plate by using a silver paste such that current could be transmitted from the electrode of a high-voltage amplifier (Trek model 663) to the upper plate via a wire dipped in the brine. The lower glass plate was then brought into electrical contact with the other pole of the electrode by using a cable and electroconductive glue. The lower glass plate was placed on the metallic plate whose temperature was maintained at 30.0 °C with an accuracy of 0.1 °C by the ceramic heaters and a controller. On the other hand, the temperature of the upper plate could not be controlled, and so the experimental data were slightly influenced by the room temperature (24 °–28 °C). Although the temperature of the bottom plate was higher than that of the upper plate by $2^\circ \sim 6^\circ$C, no thermal convection, i.e., the Rayleigh-Bénard convection, was observed, which is quite natural by the following reason: Whereas the threshold of the temperature difference for the thermal convection in homogeneously aligned MBBA molecules, that is, very close to the flow-aligned situation in the present system, is 15.5 °C

for thickness of 0.5 mm [21], the maximum of temperature difference in the present system is only 6 °C for 0.1 mm. The view field of the sample was illuminated by a fiber optic illuminator, and the sample was observed through the lower glass plate with a video microscope (Mitsutoyo VMU-H) and monochrome high-speed camera (Photoron Fastcam-R2) with spatial and intensity resolutions of 512 × 480 pixels and a grayscale of 256, respectively. The observed image of the transmitted light passing through the sample is the mixture of the director pattern "texture," which is generally used in the liquid crystal research and the shadowgraph image of EHC [2,22]. The distance between the center of rotation and the center of the view field was approximately 25 mm and the size of the view field was 190 × 178 μm.

An electric field was applied through a synthesizer (NF Corporation WF1944) and the high-voltage amplifier. Since sparks were generated above 320 V, the voltage V was varied stepwise from 0 to 310 V. The voltage amplitude is expressed in terms of the root-mean-square value throughout the remainder of this paper.

In each experimental run, shear stress measurements began 30 s after applying the electric field and about 480 data points were obtained in a run. The apparent viscosity was then evaluated by using the average value of the measurements. The shear rate $\dot{\gamma}$ for a fluid flowing between two parallel plates with gap d, one moving at a constant speed and the other stationary, is defined by $\dot{\gamma} = v/d$, where v is the velocity of the moving plate. In the present system, the shear rate depends on the distance from the center of the disk. The shear rate then was evaluated at the edge of the rotating disk (in the present case, $r = 30$ mm), and the shear stress σ was calculated from the measured torque under a Newtonian fluid assumption because parallel plates were used in the experiments.

III. RESULTS AND DISCUSSION

A. Frequency dependence of EHC threshold voltage

The EHC threshold voltage $V_{\rm th}$ is well known to increase with the increase of frequency f. Therefore, before commencing rheological measurements, we evaluated the frequency dependence of $V_{\rm th}$ by using a fixed glass cell. An MBBA sample was sandwiched between two parallel glass plates coated with a transparent electrode. The thickness and size of the cell were 30 μm and 2 × 3 cm, respectively. Homogeneous alignment of the nematic director was achieved by rubbing a polyimide (Nissan Chemical Industries, SUNEVER SE-410) coating onto the glass substrates. An ac voltage was then supplied by the synthesizer combined with a high-speed amplifier (FLC Electronics F10A). We measured the time τ taken after applying V to form a striped pattern known as the *Williams domain* [1,2]. We then plotted τ^{-1} as a function of V and extrapolated to find $V_{\rm th}$ at which $\tau(V_{\rm th})^{-1}$ vanishes. As shown in Fig. 2, $V_{\rm th}$ diverges as f approaches the critical value $f_c \approx 900$ Hz. For $f = 1000$ Hz, no pattern including the chevron was observed in the measured voltage range $0 < V < 60$ V.

Since $V_{\rm th}$ notably changed at $f \approx 600$ Hz, we selected frequencies of $f = 60$, 300, 500, 600, 700, and 1000 Hz for rheological measurements.

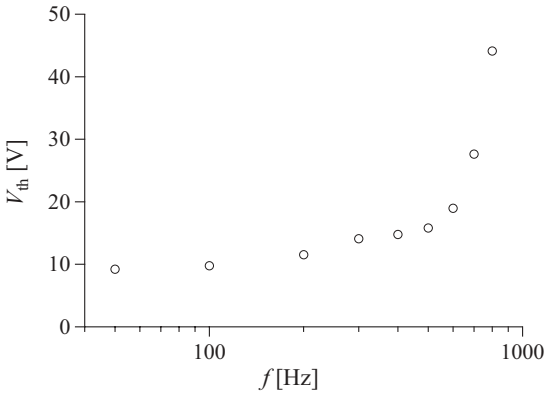

FIG. 2. Frequency dependence of EHC threshold voltage $V_{\rm th}$ in the fixed cell.

B. Rheology measurements

We first measured the dependence of the apparent viscosity η on the applied voltage for various shear rates $\dot{\gamma}$ while fixing $f = 60$ Hz. As shown in Fig. 3, for all shear rates, $\eta(V)$ increases under low voltages and then decreases under high voltages. Above 100 V for $\dot{\gamma} = 3.93$ s^{-1} and above 150 V for $\dot{\gamma} = 7.85$ s^{-1} the viscosities were lower than the rheometer's measurable range. When the electric field is removed, the viscosity returns to $\eta(0)$ within 1 s. $V_{\rm peak}$ increases monotonically as the shear rate increases (Fig. 4). Moreover, for $\dot{\gamma} = 3.93$, 7.85 and 15.7 s^{-1}, note that the viscosities under high voltages are less than the minimum of the Miesowicz viscosities at 30 °C, $\eta_2 = 19.5$ mPa s [23].

Second, we measured the dependence of the apparent viscosity on the applied voltage for $f = 60$, 300, 500, 600, 700, and 1000 Hz while fixing $\dot{\gamma} = 7.85$ s^{-1}. In this experiment, the sample was also observed using the videoscope. The apparent viscosity and acquired images are shown in Fig. 5 and Fig. 6, see Supplemental Material [24], respectively. The asterisks following the applied voltage values in Fig. 6 denote

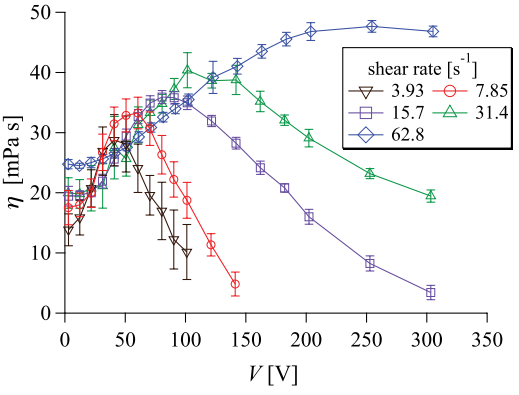

FIG. 3. (Color online) Applied voltage dependence of apparent viscosity for several shear rates. The frequency of the applied electric field is fixed at 60 Hz. For $\dot{\gamma} = 3.93$, 7.85, 15.7, and 62.8 s^{-1} at the edge $r = 30$ mm, the rotational speeds of the upper disk are 0.125, 0.25, 0.50, 1.0, and 2.0 rpm, respectively. Since data for $\dot{\gamma} = 3.93$ s^{-1} approach the rheometer's detection limit, we expect that their values are slightly less than the actual values.

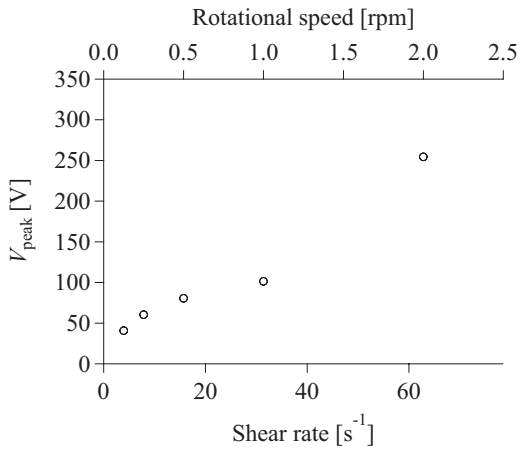

FIG. 4. Shear rate (rotational speed) dependence of the peak voltage. The frequency is fixed at 60 Hz.

the existence of EHC, and the frequency of the applied field is given on the left-hand side of each image row. For the case of $f = 1000$ Hz, as shown in Figs. 6(f-1) and 6(f-2), no characteristic pattern of EHC was observed. In the absence of an electric field, as shown in Fig. 6(g), disclinations (threadlike lines) and walls (opaque bands) stretched along the flow direction were observed. Obviously, they were generated by the flow field. Besides, the disclinations were also generated by the strong agitation flow of EHC, especially in the high-voltage conduction regime.

Let us briefly focus on the primary pattern of EHC at the voltages close to V_{th}. Since no anchoring treatment was adopted on the glass plates, the primary pattern of EHC without a shear field was not periodic stable rolls like the Williams domain but irregular rolls that fluctuate slowly as shown in Fig. 6(h). Under the shear field, both the primary pattern of EHC and its background depend on the frequency of applied voltage. In the low-frequency regime less than 600 Hz, due to the strongly deformed background consisting of the disclinations and walls generated by the shear field, no typical primary pattern of EHC was observed. For the case of $f = 60$ and 300 Hz shown in Figs. 6(a-1) and 6(b-1), it is difficult to distinguish the rolls of EHC from the background objects in spite of the fact

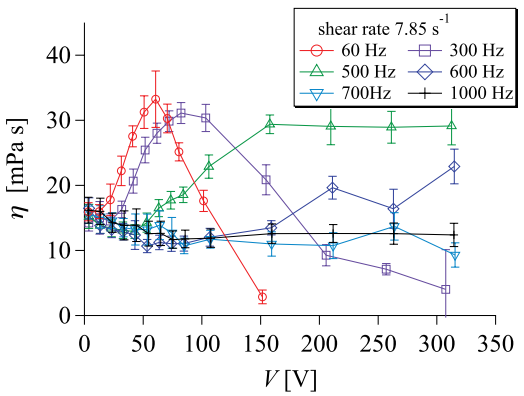

FIG. 5. (Color online) Applied voltage dependence of apparent viscosity for several frequencies. The shear rate is fixed at 7.85 s^{-1}.

that enough strength of voltages to induce EHC was applied on the system without shear flow. So the asterisks marked on Figs. 6(a-1) and 6(b-1) just mean "EHC is expected." For the case of $f = 500$ Hz shown in Fig. 6(c-1), one can see distorted rolls of EHC weakly orientated along the flow direction. On the other hand, for the cases of $f = 600$ and 700 Hz, as shown in Figs. 6(d-2) and 6(e-2), a domain of fairly regular rolls (which we named *localized Williams domain*) appeared from the wall-free background. These domains were not steady but drifting toward the flow direction. The roll-axis direction of the domains is almost perpendicular to the flow direction. Obviously, the shear flow performs the same role as the anchoring force from the glass plates (i.e., the polyimide coating with rubbing in Sec. III A). Since the localized Williams domains were observed only under $f = 600$ and 700 Hz, the electric force which aligns the director parallel to the glass plate may also play an important role to generate them. Further investigations for the formation process of the localized Williams domain are in progress. We will report it elsewhere.

Generally speaking, greater development of EHC increases the complexity of the observed image. Since the darkness of an observed image containing numerous disclinations is considered to reflect the convection complexity, we calculated the mean gray value of the observations $T(V,f)$ averaged over 2048 successive images and plotted the results in Fig. 7, where error bars denote the standard deviations. Although the voltage dependencies of the mean gray values when $f = 60$ and 300 Hz monotonically decrease, a clear change in the $T(V,f)$ curves around V_{peak} is not seen. The trends of the $T(V,f)$ curves for $f = 60$ and 300 Hz are similar to that reported by Honda *et al.* [13] for the intensity of transmitted light passing though a narrow channel under a dc field.

Before discussing the viscosity under EHC, let us consider molecular alignment in the absence of EHC [the corresponding images are shown in Figs. 6(d-1), 6(e-1), 6(f-1), and 6(f-2)]. For the sake of simplicity, we suppose the ideal director alignment defined with the Euler angles θ and ϕ in the shear field shown in Fig. 8, where the lower plate is fixed, the upper plate is moving at a constant velocity in the x direction, the velocity gradient is parallel to the z direction, and the electric field is applied along the z direction.

In the absence of an electric field, MBBA molecules are known to tilt toward the flow direction (i.e., $\phi \approx 0^\circ$ and $\theta > 0^\circ$), which is called the *flow alignment effect* [15]. According to the Ericksen-Leslie theory [15], the viscosity in the absence of an electric field is described by

$$\eta(\theta,\phi) = \tfrac{1}{2}\{(2\alpha_1\cos^2\theta + \alpha_3 + \alpha_6)\sin^2\theta\cos^2\phi + (\alpha_5 - \alpha_2)\cos^2\theta + \alpha_4\}, \quad (1)$$

where α_1-α_6 are the Leslie coefficients. The minimum and maximum values of $\eta(\theta,\phi)$ correspond to the Miesowicz viscosities $\eta_2 = \eta(90^\circ,0^\circ) = \frac{1}{2}(\alpha_3 + \alpha_4 + \alpha_6)$ and $\eta_1 = \eta(0^\circ,0^\circ) = \frac{1}{2}(-\alpha_2 + \alpha_4 + \alpha_5)$, respectively. The Leslie coefficients and the Miesowicz viscosities at 30 °C estimated from data in Ref. [23] are listed in Table I. When the director is in the xz plane ($\phi = 0^\circ$), its tilt angle in the equilibrium state θ_0 can be deduced from the relation

$$\cos 2\theta_0 = \frac{\alpha_3 - \alpha_2}{\alpha_2 + \alpha_3}. \quad (2)$$

TABLE I. Leslie coefficients and Miesowicz viscosities at 30 °C. Units are mPa s.

α_1	α_2	α_3	α_4	α_5	α_6	$\eta_1 = \frac{1}{2}(-\alpha_2 + \alpha_4 + \alpha_5)$	$\eta_2 = \frac{1}{2}(\alpha_3 + \alpha_4 + \alpha_6)$	$\eta_3 = \frac{\alpha_4}{2}$
6	−57	−0.944	65	38.2	−25.056	80.1	19.5	32.5

Substituting the values in Table I into Eqs. (1) and (2), we find that $\eta(\theta_0,0^\circ) \approx 20.6$ mPa s and $\theta_0 \approx 82.6^\circ$. Since the viscosities for $\dot{\gamma} = 3.93$–31.4 s^{-1} without an electric field are similar to $\eta(\theta_0,0^\circ)$, the flows were almost aligned for these shear rates. When the electric field along the z axis is applied to this flow-aligned configuration, θ_0 increases due to the negative dielectric anisotropy of the molecules and the apparent viscosity decreases because $\eta(\theta,0^\circ)$ is a decreasing function of θ. Since the tilt angle approaches 90° as V increases, the apparent viscosity monotonically decreases and

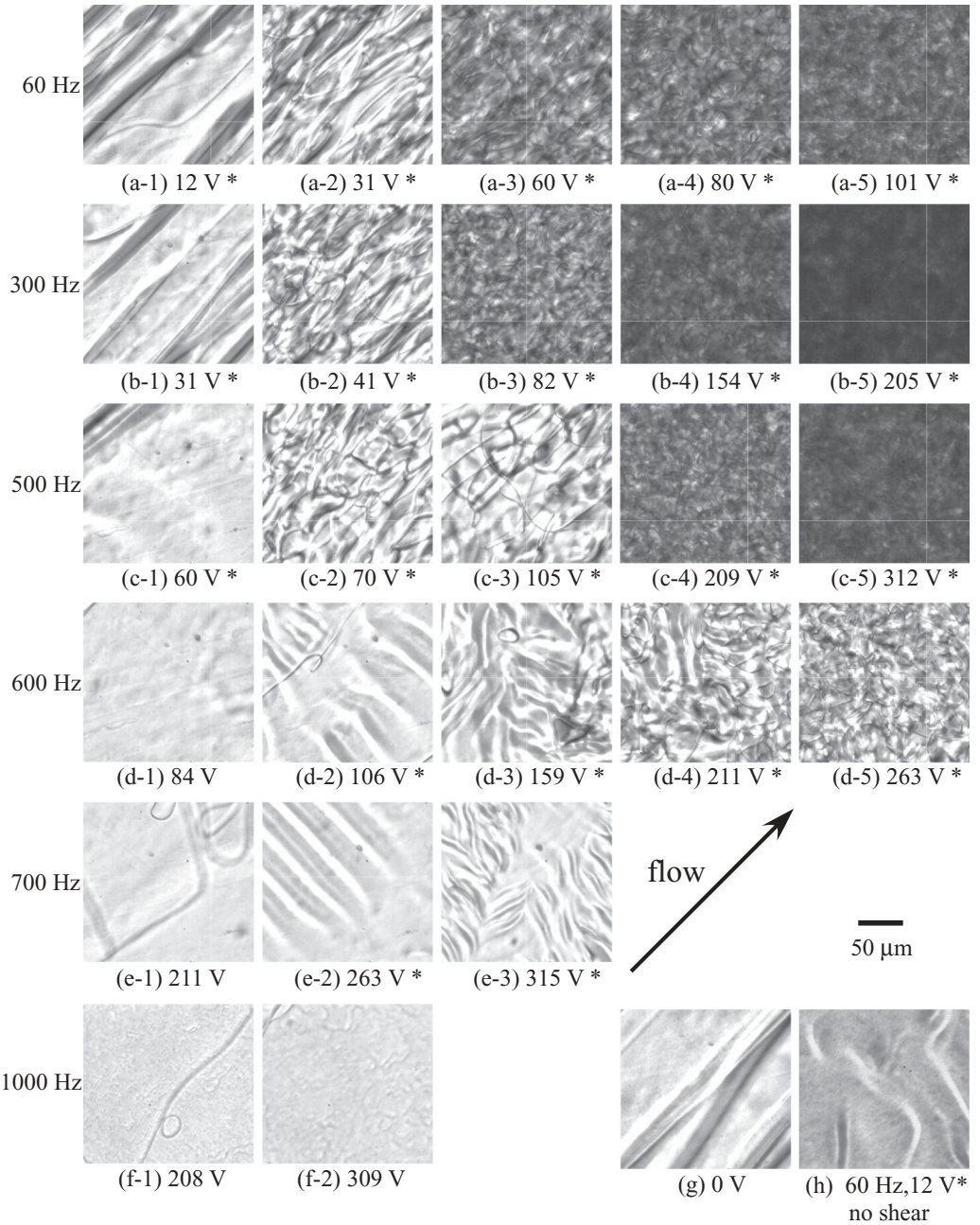

FIG. 6. The image of the transmitted light passing though the sample, see Supplemental Material [24]. Asterisks following the voltage values indicate the existence of EHC. The arrow shows the direction of flow for all photos except for (h), which is a video for 60 Hz, 12 V under no shear.

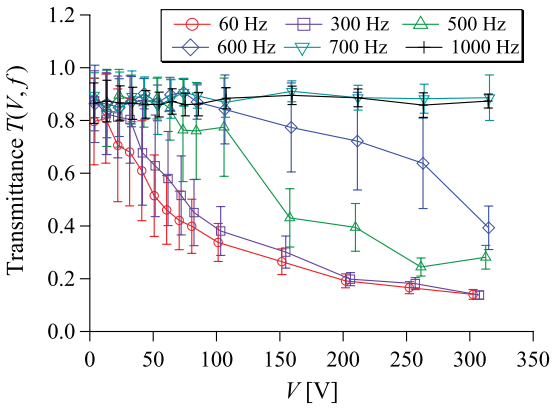

FIG. 7. (Color online) Mean gray values of observation images. Error bars denote the standard deviations.

saturates at η_2. Negita [14] observed the same behavior, i.e., the decrease and saturation in $\eta(V)$, for MBBA confined in the concentric double cylinders and also interrupted it by the increase of equilibrium tilt angle θ_0 toward 90°. Although we used parallel plates here, the decrease in viscosity for non-EHC states at 500, 600, 700, and 1000 Hz may be also explained in the same manner. In addition, it should be noted that the almost distortion-free (i.e., walls and disclinations) images of non-EHC states at 600, 700, and 1000 Hz shown in Figs. 6(d-1), 6(e-1), 6(f-1), and 6(f-2) suggest that, under the flow-aligned state, the electric force suppresses the creation of walls. Actually, when we removed the electric field, walls and disclinations came back within several seconds.

Above 20 V for 60 Hz and above 35 V for 300 Hz, the system is in a turbulent state, specifically, a DSM [1,2]. For a standard sandwich-type cell under homogenous anchoring conditions, there are two types of states, DSM1 and DSM2, distinguished by the existence of disclinations [20,25]. Whereas disclinations are not usually found in the DSM1 state, numerous disclinations exist in the DSM2 state, which reduces the sample's light transmittance. Without a shear field, the bifurcation voltage between the two states for the present rheometer-confined sample was about 29.7 V, similar to the bifurcation voltage of 31 V for a typical glass cell as reported by Kai *et al.* [20,25]. In contrast, detecting the bifurcation voltage quantitatively under a shear flow was difficult because disclinations are generated even in the DSM1 state. A qualitative judgment can be given by examining the observed images, however, and we can report with some certainty that the sample was in the DSM2 state above 40 V for 60 Hz and above 50 V for 300 Hz. On the other hand, the $\eta(V)$ curves for $f = 60$ and 300 Hz have peaks

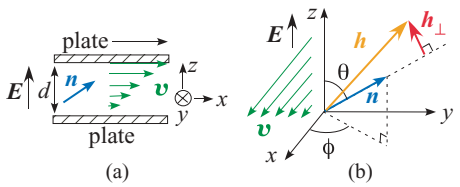

FIG. 8. (Color online) Coordinate system specifying the orientations of the director **n**, directions of the velocity **v**, and the electric field **E**. (a) x-z cross-sectional view; (b) three-dimensional view. The director is defined with the Euler angles θ and ϕ.

at $V_{\rm peak} \approx 60$ and 82 V, respectively. Therefore, the $V_{\rm peak}$ is considerably larger than the bifurcation voltage between the two DSM states.

For the cases $f = 500$ and 600 Hz, $\eta(V)$ slightly increased when $V > 50$ V and $V > 90$ V, respectively. If we applied a voltage of greater than 310 V, we would observe a decrease in $\eta(V)$. Similarly, even though an increase in $\eta(V)$ was not observed when $f = 700$ Hz, its increase and decrease can be observed if we apply a voltage exceeding 310 V, because EHC was induced at around 260 V [Fig. 6(e-2)]. Explicitly, we speculate that the apparent viscosity will generally decrease below the cut-off frequency under high voltages.

C. Spatial correlation function

To evaluate the average structure of the image of the transmitted light, we introduce a two-dimensional spatial autocorrelation function,

$$C(\mathbf{r}) = \left\langle \frac{\langle I(\mathbf{r},t)I(\mathbf{0},t)\rangle_r}{\langle I(\mathbf{0},t)^2\rangle_r} \right\rangle_t , \tag{3}$$

where $I(\mathbf{r},t)$ is the gray value of the image. Images showing this function averaged over 2048 successive observations at a frame rate 250 s^{-1} are given in Fig. 9, where the values following the applied voltages denote the minimum correlation value $C_{\rm min}$. The correlation function in each image thus varies from $C_{\rm min}$ to 1 and is expressed on a grayscale of 256 values, where black and white correspond to $C_{\rm min}$ and 1, respectively. It should be noted that the more $C_{\rm min}$ is close to 1 the more the variation of correlation function is displayed exaggeratedly in the grayscale correlation image.

Generally, the rolls of EHC coexist with the disclinations and walls. Since the the disclinations and walls are stretched along the flow direction, $C(\mathbf{r})$ forms an ellipse whose major axis is parallel to the flow direction. The exceptions are the cases shown in Figs. 9(d-2), 9(e-2), and 9(e-3) in which the localized Williams domains induced by flow alignment create striped correlation patterns. Except for these cases, the correlation function reflects both the rolls of EHC and its background objects, and the contributions from the background objects are dominant at the voltages close to $V_{\rm th}$, especially for the cases shown in Figs. 9(a-1) and 9(b-1). Above $V_{\rm th}$, the ellipticity of correlation pattern decreases as the increase of applied voltage in general. Obviously, greater development of EHC agitation flow reduces the ellipticity of the $C(\mathbf{r})$ form. For a standard sandwich-type cell under homogenous anchoring conditions, the DSM1 director is influenced by the anchoring force from the glass plates, whereas the DSM2 director remains uninfluenced. As a result, images of transmitted light in the DSM1 and DSM2 states are anisotropic and isotropic, respectively [20,25]. On the other hand, the images of the transmitted light in both states are anisotropic in the current experiments due to the shear flow. Although the ellipticity of the peak in the correlation images for DSM2 state is extremely small under high voltages, we consider it plausible that the shear field breaks the isotropic symmetry of the DSM2 state.

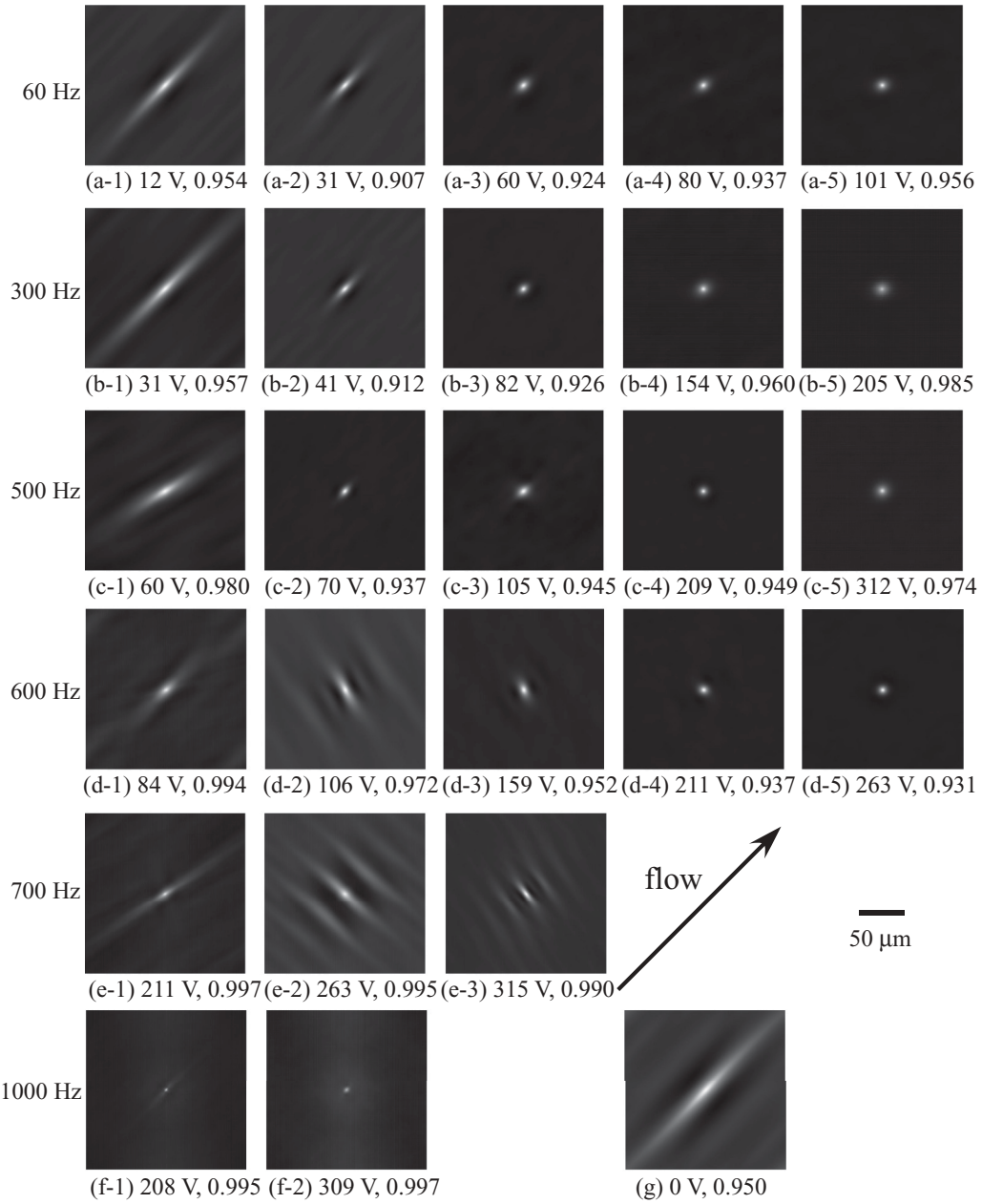

FIG. 9. Spatial autocorrelation function under shear and electric fields. Numbers following the voltage values denote minimum correlation $C_{\min}$. The correlation function thus varies from $C_{\min}$ to 1 and is expressed on a grayscale of 256 values. The arrow shows the direction of flow for all correlation images.

D. Another liquid crystal with negative dielectric anisotropy

Since EHC causes the anomalous behavior in the apparent viscosity, the same phenomenon is expected to be generally observed for nematics with negative dielectric anisotropy. To clarify this supposition, we repeated the previous experiment on Merck MLC2038, which has a dielectric anisotropy of -5.0 at 20 °C and 1 kHz. To induce EHC, we doped the MLC2038 with TBAB at a weight ratio of 0.01%. The dependence of the apparent viscosity on the applied voltage then was measured at frequencies $f = 60$, 300, 500, 700, and 1000 Hz while fixing $\dot{\gamma} = 7.85\ \mathrm{s}^{-1}$. From Fig. 10, the viscosity decreases under high voltages, and a similar frequency dependence of $\eta(V)$ is observed. Hence, the same phenomenon is quantitatively seen for MLC2038. However, the viscosity under high voltages at $f = 60$ Hz is larger than that without an electric field, which disagrees with the MBBA results.

E. Effect of electric field on the shear stress

Finally, let us discuss the effect of the electric field on the shear stress. For simplicity, we assume that the molecules are uniformly aligned as in Fig. 8. According to the

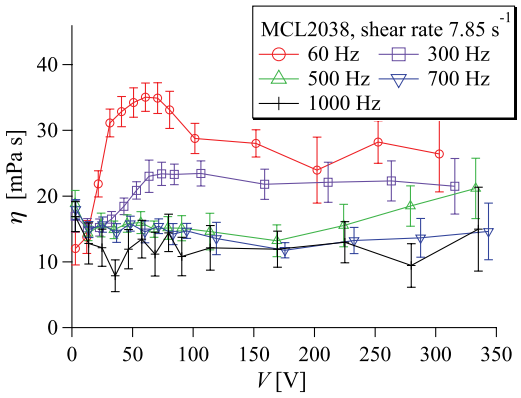

FIG. 10. (Color online) Applied voltage dependence of apparent viscosity for MLC2038.

Ericksen-Leslie theory [15], the shear stress σ_{zx} acting on the upper plate is

$$\sigma_{zx} = \frac{\dot{\gamma}}{2}\left(\alpha_4 + 2\alpha_1 n_x^2 n_z^2 + \alpha_5 n_z^2 + \alpha_6 n_x^2\right) + \alpha_2 n_z N_x + \alpha_3 n_x N_z, \tag{4}$$

$$N_x = \frac{1}{\gamma_1}\left(h_x - \gamma_2 \frac{\dot{\gamma}}{2} n_z\right), \tag{5}$$

$$N_z = \frac{1}{\gamma_1}\left(h_z - \gamma_2 \frac{\dot{\gamma}}{2} n_x\right), \tag{6}$$

$$\gamma_1 = \alpha_3 - \alpha_2, \tag{7}$$

$$\gamma_2 = \alpha_6 - \alpha_5 = \alpha_2 + \alpha_3, \tag{8}$$

where n_x and n_z are the x and z components of the director $\mathbf{n}$, respectively, N_x and N_z are the x and z components of the vector $\mathbf{N}$, which expresses the rate of change of the director with respect to the background fluid, and h_x and h_z are the x and z components of the molecular field $\mathbf{h}$. Under the Cartesian coordinate system shown in Fig. 8(b), the components of the director are given by

$$n_x = \sin\theta\cos\phi, \tag{9}$$

$$n_z = \cos\theta. \tag{10}$$

The contribution of the electric field $\mathbf{E}$ on the molecular field is then

$$h_\alpha = -\frac{\partial}{\partial n_\alpha}\left\{-\frac{1}{2}\varepsilon_0\varepsilon_\perp E^2 - \frac{1}{2}\varepsilon_0\varepsilon_a(\mathbf{n}\cdot\mathbf{E})^2\right\}, \quad (\alpha = x,y,z), \tag{11}$$

where ε_0 is the dielectric constant of the vacuum and $\varepsilon_a = \varepsilon_{//} - \varepsilon_\perp$ is the dielectric anisotropy [for dielectric constants parallel ($\varepsilon_{//}$) and perpendicular ($\varepsilon_\perp$) to the director]. Since the director is a unit vector, only the normal component of $\mathbf{h}$ with respect to $\mathbf{n}$ acts on the director in actuality. Therefore, h_x and h_z in Eqs. (5) and (6) are replaced by $h_{x\perp}$ and $h_{z\perp}$, respectively, where

$$h_{x\perp} = (\mathbf{h} - (\mathbf{h}\cdot\mathbf{n})\mathbf{n})_x = \varepsilon_0\varepsilon_a E^2\left(-n_x n_z^2\right), \tag{12}$$

$$h_{z\perp} = (\mathbf{h} - (\mathbf{h}\cdot\mathbf{n})\mathbf{n})_z = \varepsilon_0\varepsilon_a E^2\left(n_z - n_z^3\right). \tag{13}$$

Substituting Eqs. (5)–(8), (12), and (13) into Eq. (4), we finally obtain

$$\sigma_{zx} = \sigma_{zx}^{(v)} + \sigma_{zx}^{(e)}, \tag{14}$$

$$\sigma_{zx}^{(v)} = \frac{\dot{\gamma}}{2}\left\{\alpha_4 + 2\alpha_1 n_x^2 n_z^2 + \alpha_5 n_z^2 + \alpha_6 n_x^2 - \frac{\alpha_2+\alpha_3}{\alpha_3-\alpha_2}\left(\alpha_2 n_z^2 + \alpha_3 n_x^2\right)\right\}, \tag{15}$$

$$\sigma_{zx}^{(e)} = \varepsilon_0\varepsilon_a E^2 n_x n_z \frac{\alpha_3 - (\alpha_2+\alpha_3)n_z^2}{\alpha_3 - \alpha_2}. \tag{16}$$

Since $\sigma_{zx}^{(e)}$ accounts for the effect of the electric field on the shear stress, we term it the *electric stress*. Note that even though we have assumed simple shear flow, the electric stress is independent of $\dot{\gamma}$ (i.e., the flow properties) and is dependent only on the director. By utilizing the Leslie coefficients in Table I and a dielectric anisotropy of $\varepsilon_a = -0.583$ at 30 °C estimated from data in Ref. [26], the Euler angle dependencies of $\sigma_{zx}^{(v)}$, $\sigma_{zx}^{(e)}$, and σ_{zx} for the case $d = 100$ μm, $V = 100$ V, and $\dot{\gamma} = 7.85$ s^{-1} are presented as contour plots in Figs. 11(a), 11(b) and 11(c), respectively. We remark that $\sigma_{zx}^{(e)}$ is negative on the left-hand side of Fig. 11(b) and has a minimum at around $(\theta,\phi) = (30°, 0°)$. When the director is uniformly aligned along the x axis (i.e., $\theta = 90°$ and $\phi = 0°$), $\sigma_{zx}^{(e)}$ then vanishes.

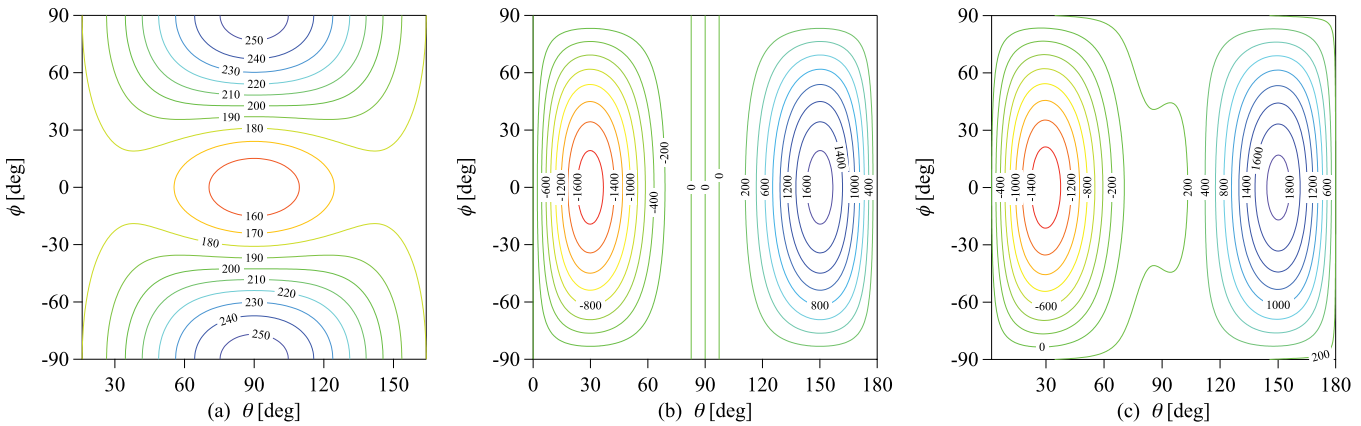

FIG. 11. (Color online) Contour plots of the shear stress for $d = 100$ μm, $V = 100$ V, and $\dot{\gamma} = 7.85$ s^{-1}: (a) $\sigma_{zx}^{(v)}$, (b) $\sigma_{zx}^{(e)}$, and (c) σ_{zx}. Values on the contour lines are expressed in units of mPa.

We thus consider that when EHC is not induced and the director is almost aligned in the x direction, the electric stress is negligible. Conversely, when EHC states exist, quantitative evaluation of the shear stress is difficult. However, the electric stress may play an important role in changing the apparent viscosity under high voltages because the electric stress is proportional to E^2. Intuitively, the electric stress in an EHC state can be roughly estimated from the average value of $\sigma_{zx}^{(e)}$, if we can measure the director distribution between the parallel plates. If we consider the probability density function for the director orientation in the sample, $P(\theta,\phi)$, and $P(\theta,\phi)$ has a broad peak around $(\theta,\phi) = (30^\circ,0^\circ)$ due to the shear flow along the x direction, the average value of $\sigma_{zx}^{(e)}$ in the DMS2 state may become negative. We postulate that, therefore, the decrease in apparent viscosity in the high-voltage DSM2 state is due to the negative contribution of the electric stress. Although it is impossible to evaluate the viscosity in the EHC states exactly, the electric stress may exist because it relates to the Maxwell stress for dielectric solids or isotropic liquids [27]. The zx components of the Maxwell stress is expressed as $\varepsilon_0\varepsilon_a E^2 n_x n_z$, though it is not exactly the same with Eq. (16). Consequently, we infer that the electric stress is a leading candidate of the origin for the decrease in apparent viscosity.

IV. SUMMARY

We have experimentally investigated the apparent viscosity of MBBA under an ac electric field. At low frequencies, the apparent viscosity is strongly influenced by EHC. As the applied voltage is increased, the viscosity first increases and then decreases, whereas EHC grows monotonically. This increase in viscosity, followed by the induction of EHC, is attributed to a disturbance of the flow-aligned director configuration whose viscosity is close to the minimum of the Miesowicz viscosities, η_2. Above the cut-off frequency, the viscosity decreases and approaches its equilibrium value. This phenomenon is explained as the homogenous alignment of the director distribution caused by the electric force and a flow alignment effect. Since a similar viscosity dependence on voltage and frequency is observed in MLC2038, we surmise that the anomalous behavior in the apparent viscosity when under an electric field is a general feature of a liquid crystal with negative dielectric anisotropy.

The decrease in viscosity is observed in the DSM2 state. To determine the origin of this decrease, we employed the Ericksen-Leslie theory in order to calculate the shear stress under the electric field. The shear stress was found to become negative under specific conditions through the contribution of the electric field. Finally, we have hypothesized that the decrease in apparent viscosity under high voltages is due to the negative contribution of the electric stress resulting from the anisotropic director distribution in the DSM2 state. However, since verification of this hypothesis by means of the present experiment is difficult, the origin of the viscosity decrease is still an open question. Further studies are, therefore, necessary.

ACKNOWLEDGMENTS

This work was partially supported by Grants-in-Aid for Scientific Research (KAKENHI), Grants No. 21540393, No. 22540416, No. 24340093, and No. 24656017 from the Japan Society for the Promotion of Science. T. Nagaya is grateful to Dr. Stefania Residori of the Institut Non-Linéaire de Nice for the many interesting discussions and acknowledges the bilateral program for scientific cooperation and scientist exchange between the Japan Society for the Promotion of Science and the Centre National de la Recherche Scientifique in France.

[1] P.-G. D. Gennes and J. Prost, in *The Physics of Liquid Crystals*, 2nd ed. (Oxford Science, New York, 1993), Chap. 5.3, pp. 230–245.
[2] L. Kramer and W. Pesch, in *Ecectrohydrodynamic Instabilites in Nematic Liquid Crystals* (Springer, New York, 1996), Chap. 6, pp. 221–255.
[3] S. Morishita, K. Nakano, and Y. Kimura, Tribol. Int. **26**, 399 (1993).
[4] I.-K. Yang and A. D. Shine, J. Rheol. **36**, 1079 (1992).
[5] R. Kishi, T. Kitano, and H. Ichijo, Mol. Cryst. Liq. Cryst. Sci. Technol., Sect. A **280**, 109 (1996).
[6] K. Negita, J. Chem. Phys. **105**, 7837 (1996).
[7] K. Negita, Mol. Cryst. Liq. Cryst. Sci. Technol., Sect. A **300**, 163 (1997).
[8] K. Negita, Liq. Cryst. **26**, 383 (1999).
[9] T. Narumi, H. See, Y. Yamaguchi, and T. Hasegawa, JSME Int. J., Ser. B **48**, 524 (2005).
[10] Y.-C. Chiang, A. Jamieson, S. Campbell, T. Tong, N. Sidocky, L. Chien, M. Kawasumi, and V. Percec, Polymer **41**, 4127 (2000).
[11] M. Cidade, C. Leal, and P. Patrício, Liq. Cryst. **37**, 1305 (2010).
[12] P. Patrício, C. Leal, L. Pinto, A. Boto, and M. Cidade, Liq. Cryst. **39**, 25 (2012).
[13] T. Honda, T. Sasada, and K. Kurosawa, Jpn. J. Appl. Phys. **17**, 1525 (1978).
[14] K. Negita, Chem. Phys. Lett. **246**, 353 (1995).
[15] P.-G. D. Gennes and J. Prost, in *The Physics of Liquid Crystals*, 2nd ed. (Oxford Science, New York, 1993), Chap. 5.1-2, pp. 198–230.
[16] P.-G. D. Gennes and J. Prost, in *The Physics of Liquid Crystals*, 2nd ed. (Oxford Science, New York, 1993), Chap. 5.3.1.2, pp. 232–232.
[17] J.-H. Huh, Y. Hidaka, A. G. Rossberg, and S. Kai, Phys. Rev. E **61**, 2769 (2000).
[18] O. L. C. Group, Mol. Cryst. Liq. Cryst. **12**, 251 (1971).
[19] H. Yamazaki, S. Kai, and K. Hirakawa, J. Phys. Soc. Jpn. **56**, 502 (1987).
[20] S. Kai and W. Zimmermann, Prog. Theor. Phys. Suppl. **99**, 458 (1989).
[21] E. Dubois-violette, E. Guyon, and P. Pieranski, Mol. Cryst. Liq. Cryst. **26**, 193 (1974).
[22] K. Kondo, M. Arakawa, A. Fukuda, and E. Kuze, Jpn. J. Appl. Phys. **22**, 394 (1983).

[23] C. Gähwiller, Mol. Cryst. Liq. Cryst. **20**, 301 (1973).

[24] See Supplemental Material at http://link.aps.org/supplemental/10.1103/PhysRevE.87.012501 for videos.

[25] S. Kai, W. Zimmermann, M. Andoh, and N. Chizumi, Phys. Rev. Lett. **64**, 1111 (1990).

[26] D. Diguet, F. Rondelez, and G. Durand, C. R. Acad. Sci., Ser. B **271**, 954 (1970).

[27] L. D. Landau, L. P. Pitaevskii, and E. Lifshitz, in *Electrodynamics of Continuous Media* (Butterworth-Heinemann, London, 1984), Chap. 2.15, 2.16, pp. 59–67.